Atmospheric Environment 333 (2024) 120672

Contents lists available at ScienceDirect

Atmospheric Environment

journal homepage: www.elsevier.com/locate/atmosenv

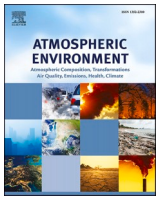

Multi-time and multi-size resolution receptor modeling to exploit jointly atmospheric aerosol data measured at different time resolutions and in multiple size classes

Federica Crova [a], Vera Bernardoni [a], Laura Cadeo [a], Silvia Canepari [b], Philip K. Hopke [c,d], Lorenzo Massimi [b], Cinzia Perrino [e], Gianluigi Valli [a], Roberta Vecchi [a,*]

[a] Department of Physics, Università degli Studi di Milano and INFN-Milano, Milan, 20133, Italy
[b] Department of Environmental Biology, Sapienza Università di Roma, Rome, 00185, Italy
[c] Institute for a Sustainable Environment, Clarkson University, Potsdam, NY 13699, USA
[d] Department of Public Health Sciences, University of Rochester School of Medicine and Dentistry, Rochester, NY 14642, USA
[e] C.N.R. Institute of Atmospheric Pollution Research, Monterotondo St., Rome, 00015, Italy

HIGHLIGHTS

- Combining traditional and advanced atmospheric aerosol data from different sampler types in receptor models is challenging.
- An expansion of the positive matrix factorization is proposed to take advantage of data measured at different time and size resolutions.
- This model applies to many datasets, providing enhanced source identification and key information for mitigation strategies.

GRAPHICAL ABSTRACT

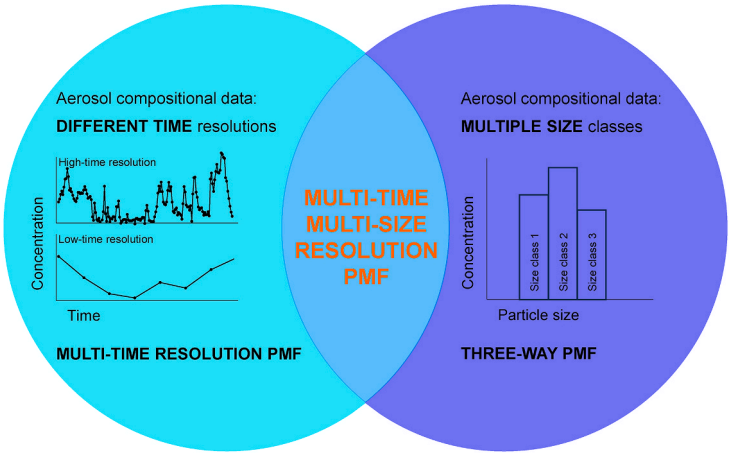

ARTICLE INFO

Keywords:
Advanced PMF
Size-segregated chemical composition
Aerosol size distribution
Multi-time analysis
Source apportionment

ABSTRACT

In the recent decades, advanced instrumentation has been developed to measure the atmospheric aerosol's physical-chemical properties with increased temporal detail and size resolution. The characterization of the atmospheric aerosol is now provided at a more detailed level. Nevertheless, it is still challenging to maximize the exploitation of such detailed information in receptor models to perform more reliable source apportionment studies. Indeed, detailed time- and size-resolved sampling can, in principle, provide additional information to better identify specific emission sources and/or atmospheric processes, but an associated complete chemical characterization is often lacking, or is provided at low time resolution by PM_X samples. To this aim, a completely

* Corresponding author. Department of Physics, Università degli Studi di Milano, via Celoria 16, 20133, Milan, Italy.
E-mail address: roberta.vecchi@unimi.it (R. Vecchi).

https://doi.org/10.1016/j.atmosenv.2024.120672
Received 8 April 2024; Received in revised form 20 June 2024; Accepted 23 June 2024
Available online 25 June 2024

novel, multi-time, multi-size resolution positive matrix factorization (MTMS-PMF) is presented. This cutting-edge receptor model is an expansion of the widely used PMF and allows the analysis of data measured at different time resolutions in multiple size classes. As output, it provides size-segregated chemical profiles and factor temporal contributions retrieved at the highest temporal resolution available in the dataset. The MTMS-PMF was implemented in a script for the Multilinear Engine ME-2 program and successfully tested on a large dataset collected in the Po Valley (Ferrara, Italy) during years 2008–2018. The dataset included aerosol chemical species measured on multistage impactor samples (8 size classes) at a low time resolution of about 1–3 weeks and daily PM_{10} samples covering almost the same sampling periods. The outputs retrieved at the higher time and size resolutions greatly strengthened the source-to-factor assignment. Moreover, the possibility to acquire information about the size distributions of atmospheric aerosol emitted by a variety of sources is highly valuable for impact assessment and for developing focused mitigation strategies aimed at addressing specific negative aerosol effects.

1. Introduction

Atmospheric aerosol particles, also referred to as particulate matter (PM), are very complex systems. Their chemical composition and size are strongly dependent on their formation mechanisms and can be altered in the atmosphere by several transformation processes. Such complexity makes the study of atmospheric PM challenging and many gaps concerning their characterization still need to be filled. However, gaining more knowledge on atmospheric PM is essential because of its effects at global scale, e.g., on cloud formation and Earth's radiative budget (e.g., IPCC, 2023), and at local scale, especially on human health (e.g., WHO global air quality guidelines, 2021). Source apportionment (SA) is a key tool to understand the atmospheric aerosol, its impacts of source-specific PM, and the development of targeted and effective mitigation strategies to improve air quality. In recent years, receptor models (RMs), and especially the positive matrix factorization (PMF) developed by Paatero and Tapper (1994), are the most commonly used models to perform SA studies (Belis et al., 2019; Hopke, 2016; Hopke et al., 2020). RMs exploit the physical-chemical PM characterization at the receptor site. In routine sampling campaigns (e.g., in air quality monitoring stations), they are generally applied to compositional data from integrated (i.e., all particles smaller than a certain size) PM_X size fraction (PM_{10}, $PM_{2.5}$, etc.) samples collected on filters, typically with a time resolution of 24 h. Filter-based measurements usually allow the collection of sufficient PM mass to achieve a complete chemical characterization of the main chemical compounds and trace species. Alternatively, advanced instrumentation has been implemented in the last decades to achieve PM data at high-time resolution, in different size classes, or both (e.g., D'Alessandro et al., 2003; Furger et al., 2020; Jayne et al., 2000; Järvinen et al., 2014; Maenhaut et al., 1996; Marple et al., 1991; Ng et al., 2011). The high temporal detail allows to capture the fast processes that aerosol particles are subjected to in the atmosphere and to distinguish sources active in specific hours of the day or episodic (e.g., Bernardoni et al., 2011; Dai et al., 2020, 2021; Kim et al., 2022; Sofowote et al., 2021; Wexler and Johnston, 2008). Size-segregated PM samples allow to study how PM properties are distributed over the size and to identify the formation processes by which the collected particles originated (e.g., Bernardoni et al., 2017; Canepari et al., 2019; Maenhaut et al., 2005; Navarro-Selma et al., 2022; Salma et al., 2005).

Although in field campaigns it is more and more common to have in parallel filter-based samplers and more advanced instrumentation, it is still challenging to combine data obtained from different types of sampling systems in traditional RMs. To address this issue, advanced RM approaches have been developed in recent years to deal with different types of data. The advanced multi-time resolution PMF was implemented by Zhou et al. (2004) in the Multilinear Engine ME-2 program (Paatero, 1999) as an expansion of the traditional PMF approach. This approach was developed to input data measured at different time resolution in the model, so that the more complete chemical characterization provided by the low-time resolution samples could be exploited together with high temporal resolution information available on specific species. This model allows obtaining as output the temporal pattern of aerosol emission source at the highest temporal resolution available in the dataset (see e.g., Crespi et al., 2016; Crova et al., 2024; Forello et al., 2019, 2020; Kuo et al., 2014; Liao et al., 2015; Mooibroek et al., 2022; Ogulei et al., 2005; Sofowote et al., 2018, 2021, 2023; Srivastava et al., 2019).

However, size-segregated data cannot be exploited in this model as formulated. Concerning size-segregated data, advanced three-way (sometimes also referred to as "3-D") PMF was proposed by Peré-Trepat et al. (2007) to use as input data measured in different size classes (e.g., collected by multistage impactors). This model was also implemented in the ME-2 program. Through this approach, emission sources are better resolved, and size-segregated chemical profiles of the sources can be retrieved (see e.g., Bernardoni et al., 2017; Karanasiou et al., 2009; Li et al., 2013; Liu et al., 2018; Shi et al., 2015; Tian et al., 2016, 2021; Ulbrich et al., 2012). However, if data in integrated PM_X size classes are available, they cannot be exploited at the same time in the three-way PMF even if they are usually much better chemically characterized than the size-segregated ones. In addition, size-segregated samples are often collected in large time intervals (even greater than 24 h) since the particulate mass amount on each impaction stage can be not enough to guarantee a robust retrieval of concentration values (see e.g., Canepari et al., 2019). Critically, the information about the temporal detail is lost.

To overcome these limitations, we developed a script for the ME-2 solver to implement the completely novel multi-time and multi-size resolution PMF (referred in the following to as MTMS-PMF), which is a combination of the multi-time resolution PMF and three-way PMF. It allows the input of data measured with different time resolutions and in different size classes. Moreover, both size-segregated data and PM_X data can be inserted at the same time in the model. In this way, the amount of information exploited is maximized. As an original output, in addition to size-segregated chemical profiles, the MTMS-PMF provides high time resolution temporal contributions of the detected emission sources. The size distributions of the PM emissions retrieved at a receptor site constitute highly valuable knowledge for developing focused mitigation plans to address specific negative impacts (e.g., controlling sources that emit ultra-fine particles containing specific harmful compounds for human health). Additionally, the detailed data obtained at both high time and size resolutions can significantly support the source-to-factor assignment process.

This paper presents the MTMS-PMF method through an application on a large dataset collected in the Po Valley (Italy), one of the most polluted sites in Europe due to intense anthropogenic emission sources and weak atmospheric dilution. This dataset included size-segregated samples with time resolutions ranging from about 1 to 3 weeks and daily PM_{10} samples and allowed to test the MTMS-PMF for the first time.

2. Materials and methods

2.1. The multi-time and multi-size resolution PMF

The MTMS-PMF was developed by expanding the multi-time resolution PMF (Zhou et al., 2004) with the three-way PMF (Peré-Trepat

et al., 2007). Details on these two modelling approaches can be found in Sections S1 and S2 of the Supplementary Material file. In the MTMS-PMF, the main equation of the multi-time resolution model (Equation S1) is modified by considering that samples can be measured in different size classes. To account for the time and size of a sample, each sample s in the input data matrix $\boldsymbol{X}$ (matrix element x_{sj} representing the input concentration of the chemical species j measured in the sample s) is associated with a start size class d_{s1} and an end size class d_{s2}. Similar to the concept of time units (i.e., the shortest time interval in the dataset) used in the multi-time resolution PMF (see Section S1), d_{s1} and d_{s2} are expressed in terms of size units. The size unit indicates one of the bins of the finer size fragmentation available in the dataset. To illustrate this concept, let us suppose having a dataset composed by PM_{10} daily samples and size-segregated samples collected with a time resolution of 1 week by a 3-stage cascade impactor in the following three size classes: below 1 μm, 1–2.5 μm, and 2.5–10 μm. It is easy to understand that the time unit characterizing this dataset is 1 day. Concerning the size unit, the integrated size fraction PM_{10} can be seen as fragmentated into the three size classes in which the size-segregated samples were collected. Then, each size class corresponds to one size unit. Consequently, size-segregated samples collected in the first stage (size below 1 μm) will be characterized by $d_{s1} = d_{s2} = 1$; the ones collected in the second stage (1–2.5 μm) will be associated with $d_{s1} = d_{s2} = 2$; finally, the ones collected in the last stage (2.5–10 μm) will have $d_{s1} = d_{s2} = 3$. All the PM_{10} samples will be associated with $d_{s1} = 1$ and $d_{s2} = 3$ since their size class can be interpreted as the union of the three smaller size intervals.

Hence, the main equation of the MTMS-PMF can be written as:

$$x_{sj} = \sum_{k=1}^{n_p} \left(\frac{1}{t_{s2} - t_{s1} + 1} \sum_{i=t_{s1}}^{t_{s2}} g_{ik} \right) \left(\sum_{d=d_{s1}}^{d_{s2}} f_{djk} \right) \eta_j + e_{sj} \quad (1)$$

The matrix $\boldsymbol{X}$ has the same dimensions $n_s \times n_2$ as in the multi-time resolution PMF ($s = 1, \ldots, n_s$; $j = 1, \ldots, n_2$) and the index s runs over all the samples in the dataset that can be measured at different time resolutions and/or in different size classes. The matrix $\boldsymbol{X}$ is decomposed into the matrices $\boldsymbol{F}$ (chemical profiles) and $\boldsymbol{G}$ (temporal contributions) of the n_p unknown independent factors, plus the modelling residual matrix $\boldsymbol{E}$. t_{s1} and t_{s2} are the start and end time of each sample s expressed in terms of time units. η_j is the adjustment factor to account for the species j measured at different time resolutions by different analytical techniques or samplings. The main difference between Equation (1) and Equation (S1) is matrix $\boldsymbol{F}$, which in this model is a size-segregated (3D) matrix with a similar structure as that introduced in the three-way PMF (see Section S2). Here, the matrix $\boldsymbol{F}$ has dimensions $n_3 \times n_2 \times n_p$, where n_3 is the total number of size units (in the previous example, $n_3 = 3$), and f_{djk} represents the concentration of the species j in the size class d of the k factor. The matrix $\boldsymbol{F}$ can be seen as a sequence of n_p layers, where each layer with dimensions $n_3 \times n_2$ represents the size-segregated chemical profile of each factor k. For samples with a size length larger than one size unit, the concentration of the species j is given by the sum of the size-segregated concentrations in the size units included in the size interval $[d_{s1}, d_{s2}]$. In this way, it is possible to insert in this model integrated PM_X data and size-segregated data measured in size classes whose union matches the PM_X size interval. Equation (1) is then solved for all x_{sj} by the ME-2 program by minimizing the object function Q given by the squared sum of the residuals scaled by the uncertainties provided in the input data. As in the traditional PMF approach, the factor profiles are assumed to be the same from the source to the receptor and in the MTMS-PMF model this is true for each size bin separately.

The MTMS-PMF was implemented by starting from the multi-time resolution PMF script implemented by Crespi et al. (2016) and the three-way PMF script implemented by Bernardoni et al. (2017). The possibility to implement auxiliary equations for constraints (see e.g., Paatero et al., 2014) and the bootstrap analysis to evaluate the robustness of the solution (see e.g., Norris et al., 2014) available in the above-mentioned multi-time resolution PMF script were extended to the MTMS-PMF.

The factor-to-source assignment can be performed by evaluating both size-segregated and integrated percent of species in each factor k, calculated as $f_{djk}/\sum_k f_{djk}$ (for each size class d and each species j) and $\sum_d f_{djk}/\sum_k \sum_d f_{djk}$ (for each species j), respectively. The size-segregated percent of species are of great interest since they allow to increase the selectivity of source tracers, especially when size-segregated data are available.

2.2. Description of the input dataset

2.2.1. Sampling

The dataset used to test the MTMS-PMF was composed of aerosol chemical components obtained on size-segregated samples collected with a time resolution of 1–3 weeks and parallel PM_{10} daily samples. Thorough descriptions of the datasets are given in Canepari et al. (2019, 2014), Farao et al. (2014), and Perrino et al. (2014). Briefly, sampling was conducted close to the city of Ferrara (about 130,000 inhabitants) in the eastern Po Valley, northern Italy. The sampling site was in a residential area of a western suburb of Ferrara (44°50′54.95″N, 11°33′40.36″E), which is about 50 km from the coast of the Adriatic Sea to the east, and about 150 km from the coast of the Tyrrhenian Sea to the south-west. The site is close to a major highway, to an industrial area, and is affected by many anthropogenic activities. It is well known that weak atmospheric dispersion is frequently observed in this area resulting in high levels of air pollution, enhanced formation of secondary aerosol species, and reprocessing of air masses (Crova et al., 2021(a), 2024; Vecchi et al., 2018, 2019). In the following, only the information relevant to the dataset exploited in this work will be reported.

Size-segregated samples were collected by a multistage impactor, the Micro-Orifice Uniform-Deposit Impactor (MOUDI), collecting particles in 10 size classes (<0.18 μm, 0.18–0.32 μm, 0.32–0.56 μm, 0.56–1.0 μm, 1.0–1.8 μm, 1.8–3.2 μm, 3.2–5.6 μm, 5.6–10 μm, 10–18 μm, and >18 μm). A back-up filter was employed to collect the particles <0.18 μm. In this work, a total of 20 size-segregated sample sets were used. They were collected from 2008 to 2018 in winter (January and February) and in summer (May and June), with a sampling time duration ranging from 6 to 22 days (Table 1). These samples were analyzed for their PM mass concentration by gravimetry, major ions by ion chromatography, and soluble and insoluble fractions of elements by inductively coupled plasma mass spectrometry (Canepari et al., 2006, 2010); for technical details about samplings and analytical techniques, please refer to Canepari et al. (2019). The chemical fractionation into the soluble and insoluble fractions has proven to be a very effective method to enhance

Table 1
Sampling periods of size-segregated and PM_{10} data exploited in this work.

Season and year	Size segregated sampling periods	PM_{10} sampling periods
Winter 2008	22 January – 31 January	10 January – 7 February
Summer 2008	29 May – 7 June	30 May – 27 June
Winter 2009	13 January – 19 January	14 January – 11 February
Summer 2009	27 May – 5 June	27 May – 25 June
Winter 2010	12 January – 19 January 26 January – 2 February	13 January – 11 February
Summer 2010	2 June – 10 June	26 May – 24 June
Winter 2011	13 January – 26 January 26 January – 7 February	13 January – 11 February
Summer 2011	31 May – 14 June 14 June – 28 June	1 June – 30 June
Winter 2012	12 January – 25 January	11 January – 12 February
Summer 2012	30 May – 11 June 15 June – 28 June	30 May – 30 June
Summer 2013	30 May – 19 June	30 May – 19 June
Winter 2014	9 January – 26 January	9 January – 29 January
Summer 2014	5 June – 21 June	5 June – 25 June
Winter 2015	9 January – 22 January	9 January – 31 January
Winter 2017	16 February – 9 March	17 February – 17 March
Winter 2018	11 January – 30 January	11 January – 1 February

the source traceability of elements (Canepari et al., 2009). Indeed, elements in the soluble fraction are generally more abundant in fine PM typically generated by combustion and by gas-to-particle transformation processes, while elements in the insoluble fraction contribute mostly to coarse PM generated by mechanical processes (such as abrasion, erosion, and resuspension).

In almost contemporaneous periods (Table 1), daily PM_{10} samples were collected on PTFE and quartz-fiber filters and characterized for their PM mass concentration by gravimetry, macro-elements by X-ray fluorescence, major ions by ion chromatography, soluble and insoluble fractions of elements by inductively coupled plasma mass spectrometry as for size-segregated samples, and elemental and organic carbon (EC and OC) by thermo-optical analysis; for technical details about samplings and analytical techniques, please refer to Canepari et al. (2014) and Perrino et al. (2014).

2.2.2. Input dataset preparation

To combine size-segregated information with PM_{10} daily samples, only the size-segregated samples corresponding to size classes 1–8 were considered since stages 9 and 10 collected particles larger than 10 μm.

A selection of the available chemical species to insert into the model was performed by considering the data quality, i.e., the signal-to-noise ratio criterion (Norris et al., 2014), the presence of outliers, and the specificity of the species as effective tracers for sources that may have affected the site during the field campaigns. The selected species in common were: PM mass concentration, 7 ions (Cl^-, NO_3^-, SO_4^{2-}, Na^+, NH_4^+, Mg^{2+}, Ca^{2+}), 5 elements in the soluble fraction (Cs_s, Li_s, Ni_s, Rb_s, V_s; the notation "_s" indicates the soluble fraction), and 7 elements in the insoluble fraction (Cu_i, Fe_i, Li_i, Mn_i, Pb_i, Sb_i, Ti_i; the notation "_i" indicates the insoluble fraction). All species were checked for the agreement between the two datasets by comparing the sum of the size-segregated data over the 8 size classes and the average of PM_{10} data over the corresponding sampling periods of size-segregated samplings. Overall, the compared data followed similar patterns, with PM_{10} data systematically larger than size-segregated data of an average factor ranging from 1.3 to 2.6, depending on the species; this might be ascribed to small differences in the cut-off efficiency curves of two samplers operated in parallel. For all these species, it was decided to correct for the differences by implementing the adjustment factors in the model (see Section S1), considering daily PM_{10} data as the benchmark. K inserted in the model came from K (PM_{10} samples) and K^+ (size-segregated samples). Lastly, Al, Si, EC, and OC were available only in the PM_{10} dataset, but thanks to the flexibility of the MTMS-PMF, it was possible to insert them in the input dataset together with the other data, thus providing a more comprehensive compositional dataset. This flexibility was a great advantage since these species are very specific tracers for some emission sources, e.g., Al and Si are excellent tracers of mineral dust (see e.g., Mason, 1966) and EC is a key tracer of combustions (see e.g., Querol et al., 2013; Reid et al., 2005). Moreover, OC constitutes a large fraction of PM mass concentrations (about on average 22% in this dataset).

All the selected species were pre-treated before inputting them in the model by following the widely used approach proposed by Polissar et al. (1998). For size-segregated data, missing data were replaced with the geometric mean calculated over the related size class and season. PM mass concentrations in both datasets were downweighed by assigning them an uncertainty of 400% (Kim et al., 2003).

In conclusion, the input matrix $\boldsymbol{X}$ used for this application consisted of $n_s = 599$ samples, $n_1 = 444$ time units, $n_2 = 25$ species, and $n_3 = 8$ size units (an example is reported in Fig. S2). 50 model runs were performed for each analysis to find the solution corresponding to the global minimum of the object function Q. A regularization equation (Equation S3) was implemented to smooth the time series and avoid artificial peaks as suggested by Zhou et al. (2004). An extra-modeling error of 10% was assigned (see Section S3 for further details). The analyses were performed in the robust mode to reduce the weights of extreme values (Brown et al., 2015).

3. Results and discussion

Solutions characterized by varying number of factors, $3 \leq n_p \leq 9$, were explored. The factor-to-source assignment was performed mainly by evaluating both size-segregated and integrated percent of species and chemical profile in each factor. Also, the factor temporal pattern resolved at the resolution of 1 day were carefully analyzed to support the factor-to-source assignment.

After 50 convergent runs, the 8-factor base-case solution corresponding to the lowest Q value (12,792) was chosen as the most physically meaningful, and the factors were assigned to biomass burning (BB), traffic (TR), nitrate (NI), sulfate and heavy oil combustion (SHO), processing of building materials (BM), soil and road dust (SR), fresh sea salt (FS), and aged sea salt (AS). A lower number of factors resulted in ambiguous chemical profiles and mixing of sources, while in the 9-factor solution the BB factor divided into two factors without a clear physical meaning. Further details about the physical robustness of the solution are reported in Section S4.

The 8-factor base-case solution represented a physically consistent representation of the major aerosol emission sources affecting the considered site. Nevertheless, the possibility to apply constraints was implemented in the MTMS-PMF to explore rotated solutions and to possibly improve the chemical profiles of some factors. The constraints were applied to the BB, TR, and SHO factors (for a total of 19 additional auxiliary equations). Their application enhanced the physical meaning of the chemical profiles without significantly affecting the source apportionments and increased the Q value by about 8%, which is considered still acceptable according to the literature (Paatero et al., 2002; Paatero and Hopke, 2008). Therefore, the constrained solution was chosen as the most reliable. In the following discussion, the full description of the factors is reported as well as the motivation of the applied constraints.

The BB factor showed high percent values of Cs_s, Rb_s, Pb_i, and K especially in the size classes below 1.8 μm. Such species are reported in the literature as tracers of biomass burning emissions (Belis et al., 2011; Canepari et al., 2019; Massimi et al., 2020; Pio et al., 2022). For the species inputted to the model available only in the integrated PM_{10} fraction (Al, Si, EC, and OC in this dataset; see also Fig. S2), size-distributions are provided also for these variables as output by the model (see Tables S2–S9). Nevertheless, due to the lack of real information about size distributions in input, the result is a uniform spread of concentrations into the different size-classes that is not physically meaningful and will not be included in the discussion of the results. Hence, only the integrated percent of species and chemical profile will be shown in the Fig. 1a and b for these species.

Among all the factors, the BB factor showed the highest percent values for Cs_s, which can be considered as tracer for these emissions (Canepari et al., 2019; Massimi et al., 2020). However, a certain amount of Cs_s was spread also in the profiles of the NI and TR factors. Thus, a pulling-up constraint was applied to Cs_s in all the size classes of the BB factor chemical profile. The constrained solution presented much higher values of Cs_s in the BB profile (integrated percent of species from 42% in the base-case to 86% in the constrained solution). This constraint also produced a significant increase of the concentrations and percent values of other typical tracers of biomass burning emissions (such as Rb_s, Pb_i, and K) and the NI and TR chemical profiles were more representative for those factors. In the final constrained solution, the BB factor is overall the largest contributor to OC (35%) and the second largest contributor to EC (28%). The PM mass distribution is concentrated in the finer size classes, with the maximum value apportioned to the 0.32–0.56 μm fraction. This result is consistent with biomass burning particles being emitted in combustion processes and emissions which are typically in the accumulation mode (Bernardoni et al., 2017). The temporal contributions are substantially higher during winter months (Fig. 2). This

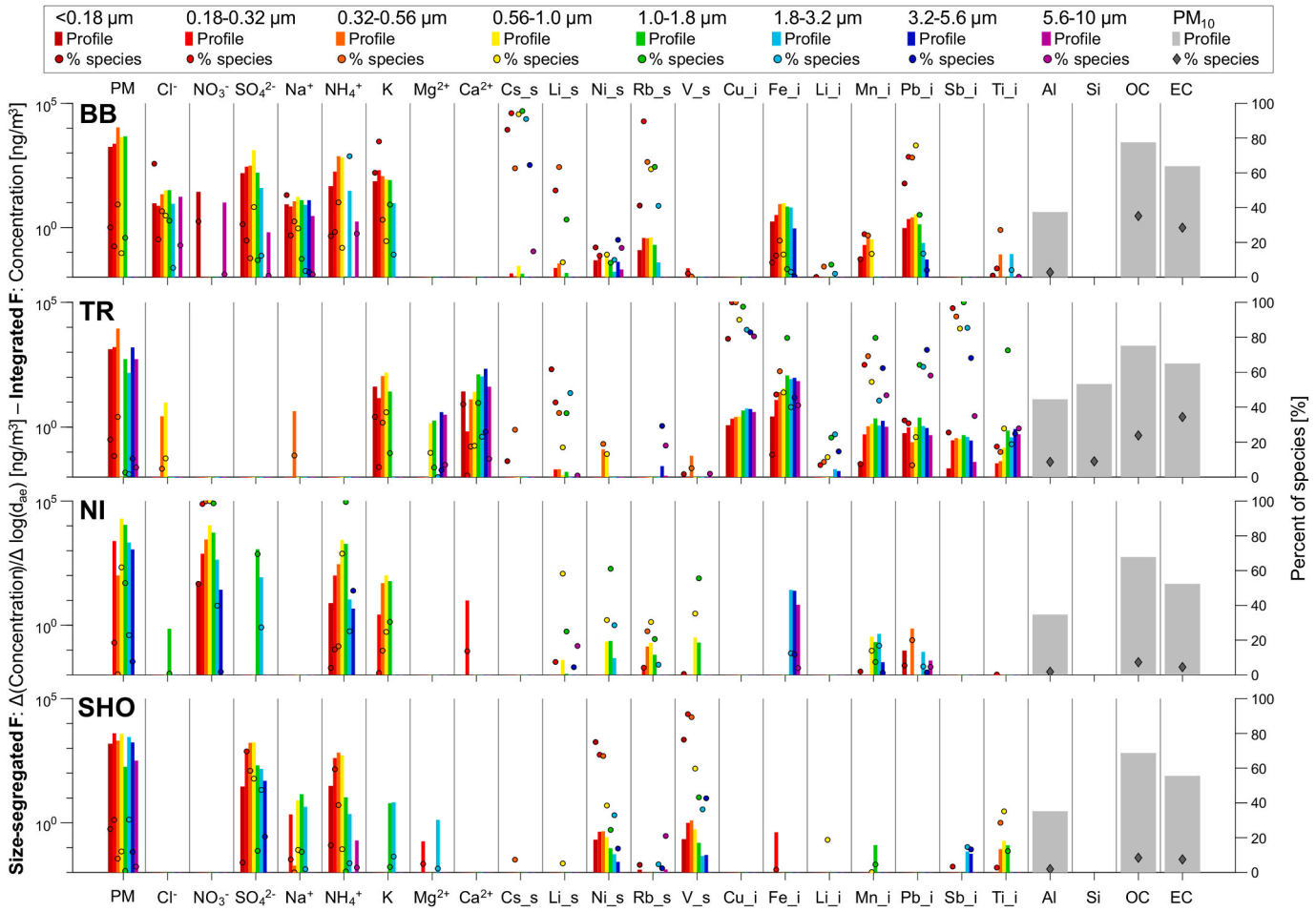

Fig. 1a. Factor chemical profiles and percent of species retrieved in the final constrained solution (first 4 factors). For PM mass concentration, ions, soluble and insoluble elements, size-segregated data are reported (chemical profile concentrations represented as discrete size distributions); for Al, Si, OC, and EC (i.e., the species available only in the PM_{10} dataset), integrated data are reported.

factor is the largest contributor to PM concentrations in winter in the size classes <0.18 µm and 0.32–0.56 µm (Fig. 3), and overall is the second largest contributor to PM_{10} integrated mass concentrations (about 22%). Its contribution drops in the summer. This difference agrees with biomass burning being mainly associated to residential heating in the Po Valley (Marigo et al., 2022; Scotto et al., 2021).

The TR factor accounted for the largest source of many elements in the insoluble fraction, i.e., Cu_i, Sb_i, Mn_i, Fe_i, and Pb_i, with contributions in the profile generally higher in the largest size classes. These species are typically associated with non-exhaust traffic emissions, where the emitted particles are formed by the wear of the mechanical components of the vehicles (Grigoratos and Martini, 2014; Pant and Harrison, 2013; Pio et al., 2022; Thorpe and Harrison, 2008). Quite large contributions in the profile are provided by Ca^{2+} and Ti_i especially in the coarser fractions, which can be associated with road dust resuspended by the moving vehicles or by asphalt wear (Amato et al., 2009; Casotti Rienda and Alves, 2021 and references therein cited). Since a non-negligible fraction of Cu_i affected the SHO profile, to explore further the solution Cu_i was pulled up maximally in all size classes in the TR factor. The constrained solution showed increased concentrations and percent values of Cu_i in the TR factor and its removal from the SHO factor. Additionally, other species considered tracers for traffic emissions, e.g., Sb_i (Varrica et al., 2013), increased in the TR profile. In the final constrained solution, the TR factor is the highest contributor to EC (34%) and the second highest contributor to OC (24%), which likely originated by tailpipe emissions (Querol et al., 2013; Viana et al., 2008). The PM mass size distribution has the largest peak in the size fraction 0.32–0.56 µm like the BB factor, suggesting that this part of mass derives from combustion processes ascribable to exhaust emissions. However, the contribution in the coarser fractions (especially in the size range 3.2–5.6 µm) was not negligible, likely associated with non-exhaust emissions. The contributions of this factor were lower in summer (Figs. 2 and 3). The seasonal difference can be explained by considering the enhanced mixing layer heights and the closure of schools and other commercial activities during summer.

The NI factor has percent values of NO_3^- close to unity in the size classes from 0.18 to 1.8 µm and very large values also for NH_4^+; these two species have very similar size distributions and are the main contributors to the profile (Fig. 1a). These observations suggest the presence of ammonium nitrate. Indeed, the highest percent values of NO_3^- and NH_4^+ are related to particles in the accumulation mode in the size classes 0.56–1 µm and 1–1.8 µm and the mean ratio NO_3^-/NH_4^+ in these bins is 3.4, which is consistent with the stoichiometric expected value. The mass contribution of this factor dominates PM_{10} integrated concentrations during winter (32%, Fig. 3), especially in size fractions between 0.56 and 3.2 µm and drastically decreases in summer (3%, see also Fig. 2), consistently with the well-known shift of the atmospheric equilibrium of ammonium nitrate to its gaseous precursors with enhanced temperatures (Seinfeld and Pandis, 2006). The PM mass size distribution reaches the maximum around 1 µm that is typical of cloud/fog processing of secondary inorganic aerosols (Bernardoni et al., 2017; Hinds, 1999; Maenhaut et al., 2005; Salma et al., 2005; Seinfeld and Pandis, 2006).

The SHO factor is characterized by high percents of V_s and Ni_s

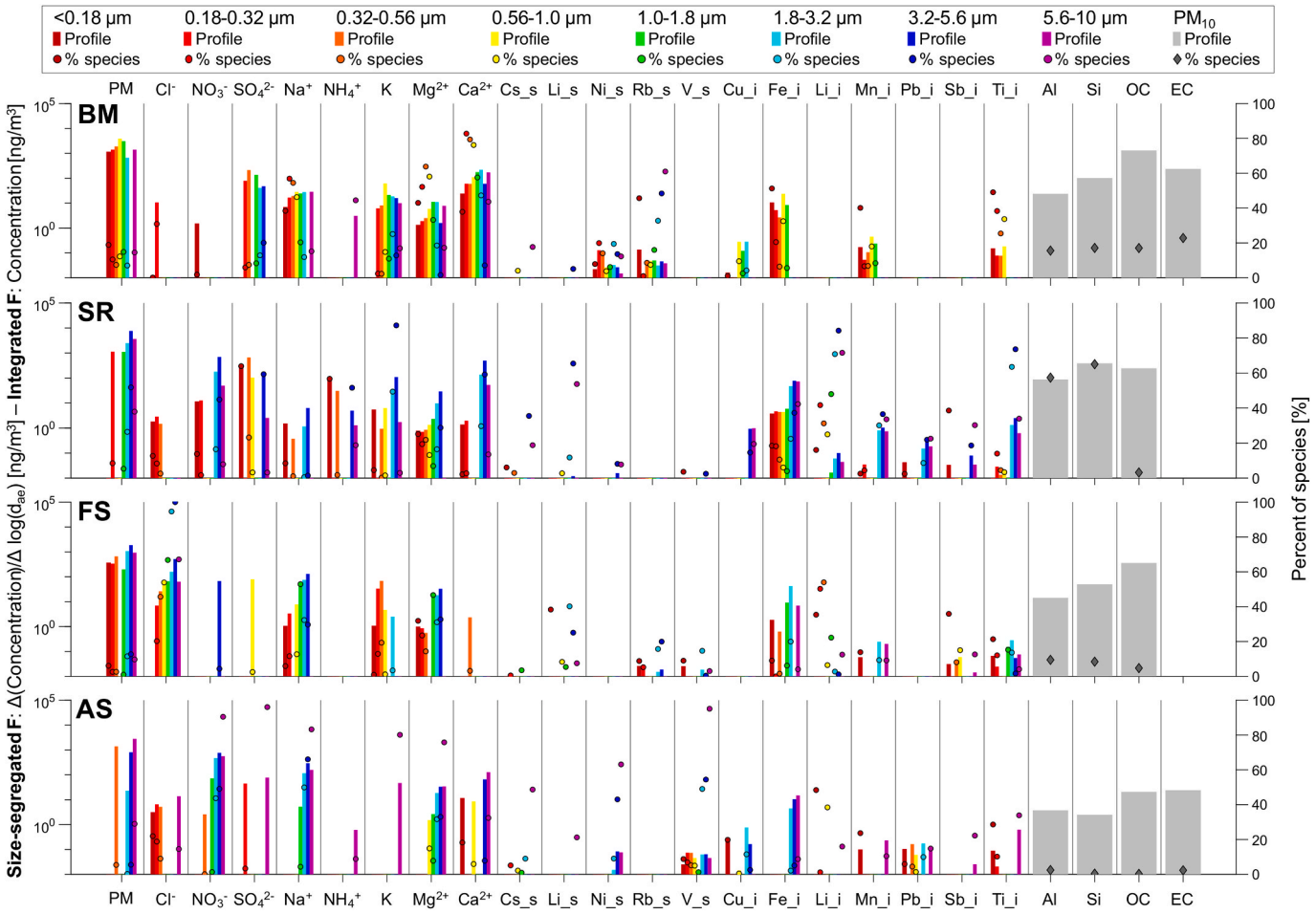

Fig. 1b. Factor chemical profiles and percent of species retrieved in the final constrained solution (last 4 factors). For PM mass concentration, ions, soluble and insoluble elements, size-segregated data are reported (chemical profile concentrations represented as discrete size distributions); for Al, Si, OC, and EC (i.e., the species available only in the PM_{10} dataset), integrated data are reported.

especially in the size classes below 1 μm. SO_4^{2-} and NH_4^+ also have quite high percent values in the finer classes and are the major contributors in the profile (Fig. 1a). V_s and Ni_s are typical tracers of heavy oil combustion associated mainly to ship and industrial emissions (Becagli et al., 2012; Bove et al., 2014; Viana et al., 2014). The large amount of SO_4^{2-} and NH_4^+ is partially ascribable to secondary ammonium sulfate. However, marine diesel emissions also contain primary sulfate given the cooling during the power stroke and the high sulfur content of marine diesel fuel (Agrawal et al., 2008a, 2008b, 2009, 2010). This factor had zero contribution to NO_3^- except for the coarser size classes 1.8–3.2 μm, 3.2–5.6 μm, and 5.6–10 μm, but no other cation was detected in this size range; thus, NO_3^- was pulled down maximally in these size classes. The constrained solution showed zero concentration of NO_3^- in all the size classes, while an increased amount of NO_3^- was found in the coarser size classes of the AS factor chemical profile, which is the only factor having non negligible contribution of NO_3^- in the coarse fraction also in the base-case solution. Finding ammonium sulfate and tracers of heavy oils together in a chemical profile is very common especially in port sites (see e.g., Pietrodangelo et al., 2024; Via et al., 2023), since heavy oils are extensively used in marine diesel engines and are an important source of sulfur (Hopke et al., 2020). However, the site here investigated is not on the coast. Therefore, these observations suggest that this factor may be associated with the transport of air masses which passed over port/-marine sites. To further support this assumption, the back-trajectories of the air masses related to the most relevant peaks in the time contribution (Fig. 2) occurring on the days 24 June 2008, 23 June 2011, and 2 June 2012 (Fig. S6) were calculated using the Hybrid Single-Particle Lagrangian Integrated Trajectory HYSPLIT model (Stein et al., 2015). It can be observed that the air masses are coming from the south-west direction and passed over the northern part of the Tyrrhenian Sea, which is highly affected by marine traffic (Bigi et al., 2017). The PM mass size distribution of this factor has its larger contribution in the finer classes with an evident double mode due to secondary ammonium sulfate (Hinds, 1999; Seinfeld and Pandis, 2006) and a non-negligible contribution in the coarse fraction. The mass contribution apportioned by this factor was higher in summer (Fig. 2) and dominated in the size classes <0.18 μm, 0.18–0.32 μm, 0.56–1 μm, and 1.8–3.2 μm. This behavior can be attributed either to more intense photochemical activity producing sulfate in summer (Seinfeld and Pandis, 2006) or to an enhanced marine traffic caused by a higher number of cruise ships.

The BM factor was not straightforward to interpret. The highest percents (Fig. 1b) were retrieved for Ca^{2+} especially in the size classes between 0.18 and 1 μm; this factor accounted for the largest integrated amount of Ca^{2+} (Table S5). Calcium has been reported in the literature as marker of soil dust in coarser size fractions (Amato et al., 2016; Viana et al., 2008), industrial activities (e.g., cement, steel, and iron manufacturing production) (Lee and Pacyna, 1999; Yubero et al., 2011), and very local sources such as construction works and coal combustion (Bernardoni et al., 2011; Samara and Tsitouridou, 2000). Among these sources, the anthropogenic activities that may be related to Ca^{2+} emissions in the investigated area could be the production of building materials as well as their manufacturing and transport by industrial vehicles. The HYSPLIT back-trajectories related to the most relevant peaks in the time contribution (Fig. 2) occurring on the days 27 June

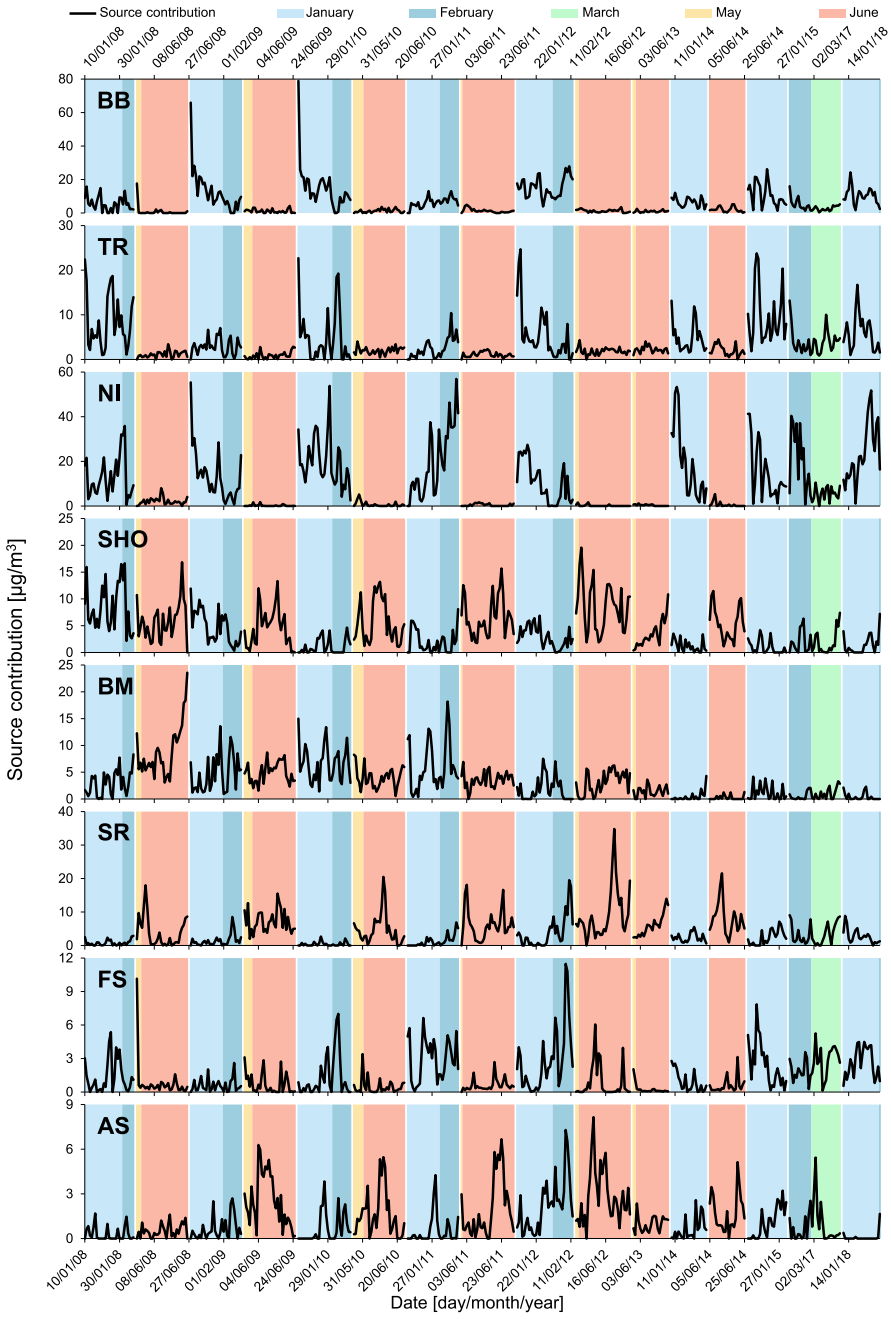

Fig. 2. Factor temporal contributions of the final constrained solution retrieved at 1 day resolution. Please note that the x-axis is not linear.

2008 and 5 February 2011 (Fig. S7) show very limited transport largely staying in the Po Valley basin, suggesting very local emission origins. Quite high percent values were also found for Mg^{2+}, Na^{+}, Fe_i, and Ti_i in the finer size classes, and for Rb_s mainly in the coarser size classes. This factor was the third largest contributor to OC (17%) and EC (23%). The high amount of EC and the PM mass size distribution of this factor mainly contributing to the finer size classes below 1 µm suggest that the particles emitted by this source originated from combustion processes, e.g., from exhaust emissions by industrial vehicles. The temporal contribution (Fig. 2) has a very peculiar decreasing pattern over the years until 2014 followed by almost stable concentrations in the remaining years, and no other factor showed a similar pattern. However, the information available until now do not give clear indications on possible abatement strategies implemented in this area for such emission sources.

The SR factor presented large percents of K, Li_i, Li_s, Ti_i, and Ca^{2+} in the coarse size fractions beyond 1.8 µm (Fig. 1b). Al and Si showed very high integrated percent values as well. These species are typically produced by mechanical processes such as abrasion and erosion of crustal material, and hence they are considered very good tracers of mineral dust (Mason, 1966; Viana et al., 2008); in addition, the presence of small contributions of heavy metals typically linked to non-exhaust traffic emissions (e.g., Sb_i, Fe_i) suggest a contribution from road dust resuspension. Consistently, the PM mass size distribution has its largest contributions in the coarser size fractions. The presence of fine SO_4^{2-} and NH_4^{+} in the profile could be ascribed to an inclusion of ammonium sulfate produced on the regional scale. The apportioned mass concentration is larger in summer and dominates in the size classes beyond 1 µm (Fig. 3), likely because the summer months are characterized generally by drier meteorological conditions that promote the resuspension of soil and road dust. Moreover, the contribution of this factor to integrated

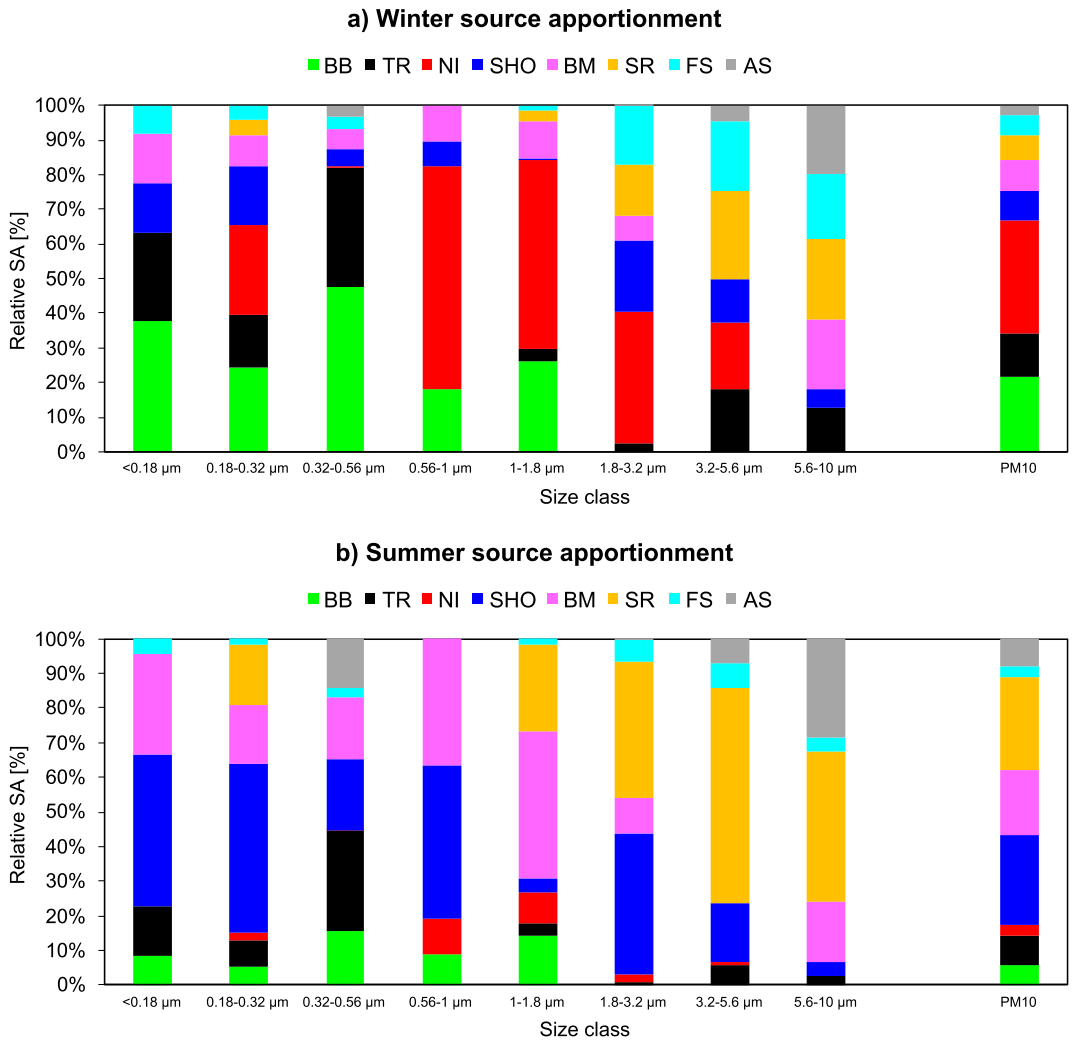

Fig. 3. Relative size-segregated and integrated (PM_{10}) source apportionment of the 8 factors in the final constrained solution.

PM_{10} concentrations in summer is overall the highest (27%).

The FS factor was characterized by very high percent values of Cl^- and by quite large values for Na^+, Mg^{2+}, and Li_s especially in the coarser size fractions over 1 µm (Fig. 1b). Such species are very common tracers of fresh sea salt, typically emitted by the breaking of surface waves (Seinfeld and Pandis, 2006). Accordingly, the PM mass size distribution of this factor has the largest contribution over 1.8 µm. Since the sampling site is not on the coast, this factor is likely associated to transport of air masses coming from the sea. To further support this hypothesis, also in this case the back-trajectories of the air masses related to the highest peaks in the time pattern (Fig. 2) occurring on the days 29 May 2008 and 8 February 2012 were retrieved by the HYSPLIT model (Fig. S8). The plots show that in both cases the air masses passed over the Adriatic Sea before reaching the site.

Finally, the AS factor showed very high percent values of various species (NO_3^-, SO_4^{2-}, Na^+, K, Mg^{2+}, Cs_s, Rb_s, and V_s) in the largest size class 5.6–10 µm. The largest contributors in the profile are NO_3^- and Na^+ in the size fractions over 1 µm. It is noteworthy that, apart a smaller contribution in the SR factor, this is the only factor where NO_3^- has a significant contribution in the coarse fraction, and is the second largest contributor of integrated NO_3^- after the NI factor. The presence of tracer species of sea salt and the negligible amount of Cl^- in the profile is a suggestion that this factor may be associated with aged sea salt, where the chloride ion was replaced by a nitrate ion (Amato et al., 2016; Canepari et al., 2019; Forello et al., 2020; Hopke et al., 2020; Seinfeld and Pandis, 2006). This reaction can easily occur when air masses coming e.g., from the Adriatic Sea mix with Po Valley air masses, which are rich in ammonium nitrate and the precursor gaseous nitric acid. The contamination of other species in the profile may be due to the ageing and mixing processes occurring during the transport of the air mass over polluted areas before reaching the receptor site.

Overall, the size distributions of the apportioned PM mass concentration and chemical components retrieved for each factor by the MTMS-PMF allowed strengthening the source-to-factor assignment. To maximize the amount of information gained, from these outputs it is also possible to retrieve the continuous size distributions by inverting the data with a suitable algorithm (e.g., the MICRON program (Wolfenbarger and Seinfeld, 1990)), and by fitting the inverted data with log-normal distributions (e.g., by following the procedure proposed by Crova et al. (2021)(b)). In this way, modal parameters of the size distributions can be assessed (an example applied on the PM mass concentration of the SR and SHO factors is given in Fig. S9) and a more detailed and comprehensive understanding of the processes and dynamics of aerosol particles in the atmosphere can be achieved.

4. Conclusions

In this work, a novel advanced receptor model MTMS-PMF was tested and applied to a real dataset by putting the information contained in the data to the maximum use. Indeed, one of the greatest strengths of the MTMS-PMF model is the possibility to combine data from different types of samples measured with different time and size resolutions. This allows

the integration of different pieces of information, i.e., in the case here presented, higher temporal detail and extended chemical composition for PM_{10} samples, along with size distributions for multistage impactor samples. The size-segregated chemical profiles retrieved as output were highly useful to understand the physical and chemical emission processes that produced the collected particles. Moreover, thanks to the flexibility of the MTMS-PMF, it was possible to insert compositional data of the major species such as carbonaceous components and crustal elements obtained from the PM_{10} data but not measured on the size-segregated samples. These features provided mass closure and allowed a much better association of the factors to aerosol emission sources. The size distributions of PM mass concentrations and specific components retrieved for each factor are key information to elaborate effective air quality management and regulatory decision-making to mitigate adverse effects of the atmospheric aerosol (e.g., to abate the sources more responsible for ultra-fine particles or harmful compounds dangerous for human health) and to enhance Earth radiation balance models. Lastly, the MTMS-PMF provided factor temporal contributions retrieved at the highest time resolution available in the dataset (i.e., 1 day). This feature allowed better understanding of the periods where the sources were most active, to obtain seasonal source apportionments, and to investigate into detail the origin of specific peaks through the HYSPLIT model (this would not be possible at all e.g., with the only size-segregated data measured at very low time resolution).

The MTMS-PMF model paves the way for many applications where field campaign data are available with different time resolutions and measured in multiple size classes, not necessarily using samples achieved with multistage impactors (which are demanding in terms of manpower and challenging for analytical quantifications). In the case-study proposed in this work, data measured with high time and low size resolutions were joined with data measured at low time and high size resolutions. Another interesting application could be joining high time and high size resolution samples with low time and low size resolution samples (e.g., hourly data collected through the streaker sampler (D'Alessandro et al., 2003) in the coarse and fine fractions with daily PM_{10} samples).

Finally, it is also important to mention that the MTMS-PMF here implemented works when the integrated size fraction matches the union of the fragmentated size classes. However, work is in progress to expand it also to cases where data are measured in size fractions covering only partially the fragmentated size classes.

Funding

This project has been carried out without any specific funding.

CRediT authorship contribution statement

Federica Crova: Writing – review & editing, Writing – original draft, Visualization, Software, Methodology, Formal analysis, Conceptualization. **Vera Bernardoni:** Writing – review & editing, Validation, Methodology, Conceptualization. **Laura Cadeo:** Writing – review & editing, Formal analysis. **Silvia Canepari:** Writing – review & editing, Validation, Investigation, Data curation. **Philip K. Hopke:** Writing – review & editing, Validation. **Lorenzo Massimi:** Writing – review & editing, Validation, Investigation, Data curation. **Cinzia Perrino:** Writing – review & editing, Validation, Investigation, Data curation. **Gianluigi Valli:** Writing – review & editing, Validation, Software, Methodology, Conceptualization. **Roberta Vecchi:** Writing – review & editing, Validation, Supervision, Methodology, Conceptualization.

Declaration of competing interest

The authors declare that they have no known competing financial interests or personal relationships that could have appeared to influence the work reported in this paper.

Data availability

Data will be made available on request.

Acknowledgements

The authors acknowledge the Università Statale di Milano for Federica Crova's PhD studentship; Herambiente S. p.A. for funding the field campaigns; Salvatore Pareti, Elena Rantica, and Tiziana Sargolini from the C.N.R. Institute of Atmospheric Pollution Research for the chemical analyses; Silvia Belmuso and Alice Forello for preliminary data reduction and source apportionment analyses.

Appendix A. Supplementary data

Supplementary data to this article can be found online at https://doi.org/10.1016/j.atmosenv.2024.120672.

References

Agrawal, H., Malloy, Q., Welch, W.A., Miller, J.W., Cocker III, D.R., 2008a. In-use gaseous and particulate matter emissions from a modern oceangoing container vessel. Atmos. Environ. 42, 5504–5510. https://doi.org/10.1016/j.atmosenv.2008.02.053.

Agrawal, H., Welch, W.A., Miller, J.W., Cocker III, D.R., 2008b. Emission measurements from a crude oil tanker at sea. Environ. Sci. Technol. 42, 7098–7103. https://doi.org/10.1021/es703102y.

Agrawal, H., Eden, R., Zhang, X., Fine, P.M., Katzenstein, A., Miller, J.W., Ospital, J., Teffera, S., Cocker III, D.R., 2009. Primary particulate matter from ocean-going engines in the Southern California air basin. Environ. Sci. Technol. 43, 5398–5402. https://doi.org/10.1021/es8035016.

Agrawal, H., Welch, W.A., Henningsen, S., Miller, J.W., Cocker III, D.R., 2010. Emissions from main propulsion engine on container ship at sea. J. Geophys. Res. 115, D23205. https://doi.org/10.1029/2009JD013346.

Amato, F., Pandolfi, M., Escrig, A., Querol, X., Alastuey, A., Pey, J., Perez, N., Hopke, P. K., 2009. Quantifying road dust resuspension in urban environment by Multilinear Engine: a comparison with PMF2. Atmos. Environ. Times 43 (17), 2770–2780. https://doi.org/10.1016/j.atmosenv.2009.02.039.

Amato, F., Alastuey, A., Karanasiou, A., Lucarelli, F., Nava, S., Calzolai, G., Severi, M., Becagli, S., Gianelle, V.L., Colombi, C., Alves, C., Custódio, D., Nunes, T., Cerqueira, M., Pio, C., Eleftheriadis, K., Diapouli, E., Reche, C., Minguillòn, M.C., Manousakas, M.-I., Maggos, T., Vratolis, S., Harrison, R.M., Querol, X., 2016. AIRUSE-LIFE+: a harmonized PM speciation and source apportionment in five southern European cities. Atmos. Chem. Phys. 16, 3289–3309. https://doi.org/10.5194/acp-16-3289-2016.

Becagli, S., Sferlazzo, D.M., Pace, G., di Sarra, A., Bommarito, C., Calzolai, G., Ghedini, C., Lucarelli, F., Meloni, D., Monteleone, F., Severi, M., Traversi, R., Udisti, R., 2012. Evidence for heavy fuel oil combustion aerosols from chemical analyses at the island of Lampedusa: a possible large role of ships emissions in the Mediterranean. Atmos. Chem. Phys. 12, 3479–3492. https://doi.org/10.5194/acp-12-3479-2012.

Belis, C.A., Favez, O., Mircea, M., Diapouli, E., Manousakas, M.-I., Vratolis, S., Gilardoni, S., Paglione, M., Decesari, S., Mocnik, G., Mooibroek, D., Salvador, P., Takahama, S., Vecchi, R., Paatero, P., 2019. European Guide on Air Pollution Source Apportionment with Receptor Models - Revised Version 802 2019, EUR 29816 EN. Publications Office of the European Union, Luxembourg. https://doi.org/10.2760/439106.

Belis, C.A., Cancelinha, J., Duane, M., Forcina, V., Pedroni, V., Passarella, R., Tanet, G., Douglas, K., Piazzalunga, A., Bolzacchini, E., Sangiorgi, G., Perrone, M.-G., Ferrero, L., Fermo, P., Larsen, B.R., 2011. Sources for PM air pollution in the Po Plain, Italy: I. Critical comparison of methods for estimating biomass burning contributions to benzo(a)pyrene. Atmos. Environ. 45 (39), 7266–7275. https://doi.org/10.1016/j.atmosenv.2011.08.061.

Bernardoni, V., Vecchi, R., Valli, G., Piazzalunga, A., Fermo, P., 2011. PM10 source apportionment in Milan (Italy) using time-resolved data. Sci. Total Environ. 409, 4788–4795. https://doi.org/10.1016/j.scitotenv.2011.07.048.

Bernardoni, V., Elser, M., Valli, G., Valentini, S., Bigi, A., Fermo, P., Piazzalunga, A., Vecchi, R., 2017. Size-segregated aerosol in a hot-spot pollution urban area: chemical composition and three-way source apportionment. Environ. Pollut. 231, 601–611. https://doi.org/10.1016/j.envpol.2017.08.040.

Bigi, A., Bianchi, F., De Gennaro, G., Di Gilio, A., Fermo, P., Ghermandi, G., Prévôt, A.S. H., Urbani, M., Valli, G., Vecchi, R., Piazzalunga, A., 2017. Hourly composition of gas and particle phase pollutants at a central urban background site in Milan. Italy. Atmos. Res. 186, 83–94. https://doi.org/10.1016/j.atmosres.2016.10.025.

Bove, M.C., Brotto, P., Cassola, F., Cuccia, E., Massabò, D., Mazzino, A., Piazzalunga, A., Prati, P., 2014. An integrated PM2.5 source apportionment study: positive Matrix Factorisation vs. the chemical transport model CAMx. Atmos. Environ. 94, 274–286. https://doi.org/10.1016/j.atmosenv.2014.05.039.

Brown, S.G., Eberly, S., Paatero, P., Norris, G.A., 2015. Methods for estimating uncertainty in PMF solutions: examples with ambient air and water quality data and

guidance on reporting PMF results. Sci. Total Environ. 518–519, 626–635. https://doi.org/10.1016/j.scitotenv.2015.01.022.
Canepari, S., Astolfi, M., Catrambone, M., Frasca, D., Marcoccia, M., Marcovecchio, F., Massimi, L., Rantica, E., Perrino, C., 2019. A combined chemical/size fractionation approach to study winter/summer variations, ageing and source strength of atmospheric particles. Environ. Pollut. 253, 19–28. https://doi.org/10.1016/j.envpol.2019.06.116.
Canepari, S., Astolfi, M., Farao, C., Maretto, M., Frasca, D., Marcoccia, M., Perrino, C., 2014. Seasonal variations in the chemical composition of particulate matter: a case study in the Po Valley. Part II: concentration and solubility of micro-and trace-elements. Environ. Sci. Pollut. Res. 21, 4010–4022. https://doi.org/10.1007/s11356-013-2298-1.
Canepari, S., Astolfi, M.L., Moretti, S., Curini, R., 2010. Comparison of extracting solutions for elemental fractionation in airborne particulate matter. Talanta 82 (2), 834–844. https://doi.org/10.1016/j.talanta.2010.05.068.
Canepari, S., Pietrodangelo, A., Perrino, C., Astolfi, M.L., Marzo, M.L., 2009. Enhancement of source traceability of atmospheric PM by elemental chemical fractionation. Atmos. Environ. 43, 4754–4765. https://doi.org/10.1016/j.atmosenv.2008.09.059.
Canepari, S., Cardarelli, E., Giuliano, A., Pietrodangelo, A., 2006. Determination of metals, metalloids and non-volatile ions in airborne particulate matter by a new two-step sequential leaching procedure: Part A: experimental design and optimisation. Talanta 69 (3), 581–587. https://doi.org/10.1016/j.talanta.2005.10.023.
Casotti Rienda, I., Alves, C.A., 2021. Road dust resuspension: a review. Atmos. Res. 261, 105740 https://doi.org/10.1016/j.atmosres.2021.105740.
Crespi, A., Bernardoni, V., Calzolai, G., Lucarelli, F., Nava, S., Valli, G., Vecchi, R., 2016. Implementing constrained multi-time approach with bootstrap analysis in ME-2: an application to PM2.5 data from Florence (Italy). Sci. Total Environ. 541, 502–511. https://doi.org/10.1016/j.scitotenv.2015.08.159.
Crova, F., Forello, A.C., Bernardoni, V., Calzolai, G., Canepari, S., Argentini, S., Costabile, F., Frezzini, M.A., Giardi, F., Lucarelli, F., Massabò, D., Massimi, L., Nava, S., Paglione, M., Pazzi, G., Prati, P., Rinaldi, M., Russo, M., Valentini, S., Valli, G., Vernocchi, V., Vecchi, R., 2024. Assessing the role of atmospheric dispersion vs. emission strength in the southern Po Valley (Italy) using dispersion-normalised multi-time receptor modelling. Atmos. Environ. 316, 120168 https://doi.org/10.1016/j.atmosenv.2023.120168.
Crova, F., Valli, G., Bernardoni, V., Forello, A.C., Valentini, S., Vecchi, R., 2021a. Effectiveness of airborne radon progeny assessment for atmospheric studies. Atmos. Res. 250, 105390 https://doi.org/10.1016/j.atmosres.2020.105390.
Crova, F., Bernardoni, V., Forello, A.C., Valentini, S., Valli, G., Vecchi, R., 2021b. Improving data analysis for size-segregated atmospheric aerosol samples. Il Nuovo Cimento C 44. https://doi.org/10.1393/ncc/i2021-21013-x.
D'Alessandro, A., Lucarelli, F., Mandò, P.A., Marcazzan, G., Nava, S., Prati, P., Valli, G., Vecchi, R., Zucchiatti, A., 2003. Hourly elemental composition and sources identification of fine and coarse PM10 particulate matter in four Italian towns. J. Aerosol Sci. 34 (2), 243–259. https://doi.org/10.1016/S0021-8502(02)00172-6.
Dai, Q., Ding, J., Hou, L., Li, L., Cai, Z., Liu, B., Song, C., Bi, X., Wu, J., Zhang, Y., Feng, Y., Hopke, P.K., 2021. Haze episodes before and during the COVID-19 shutdown in Tianjin, China: contribution of fireworks and residential burning. Environ. Pollut. 286, 117252. https://doi.org/10.1016/j.envpol.2021.117252.
Dai, Q., Liu, B., Bi, X., Wu, J., Liang, D., Zhang, Y., Feng, Y., Hopke, P.K., 2020. Dispersion normalized PMF provides insights into the significant changes in source contributions to PM2.5 after the COVID-19 outbreak. Environ. Sci. Technol. 54, 9917–9927. https://doi.org/10.1021/acs.est.0c02776.
Farao, C., Canepari, S., Perrino, C., Harrison, R.M., 2014. Sources of PM in an industrial area: comparison between receptor model results and semiempirical calculations of source contributions. Aerosol Air Qual. Res. 14 (6), 1558–1572. https://doi.org/10.4209/aaqr.2013.08.0281.
Forello, A.C., Amato, F., Bernardoni, V., Calzolai, G., Canepari, S., Costabile, F., Di Liberto, L., Gualtieri, M., Lucarelli, F., Nava, S., Perrino, C., Petralia, E., Valentini, S., Valli, G., Vecchi, R., 2020. Gaining knowledge on source contribution to aerosol optical absorption properties and organics by receptor modelling. Atmos. Environ. 243, 117873. https://doi.org/10.1016/j.atmosenv.2020.117873.
Forello, A.C., Bernardoni, V., Calzolai, G., Lucarelli, F., Massabò, D., Nava, S., Pileci, R.E., Prati, P., Valentini, S., Valli, G., Vecchi, R., 2019. Exploiting multi-wavelength aerosol absorption coefficients in a multi-time resolution source apportionment study to retrieve source-dependent absorption parameters. Atmos. Chem. Phys. 19, 11235–11252. https://doi.org/10.5194/acp-19-11235-2019.
Furger, M., Rai, P., Slowik, J.G., Cao, J., Visser, S., Baltensperger, U., Prévôt, A.S.H., 2020. Automated alternating sampling of PM10 and PM2.5 with an online XRF spectrometer. Atmos. Environ. X 5, 100065. https://doi.org/10.1016/j.aeaoa.2020.100065.
Grigoratos, T., Martini, G., 2014. Non-exhaust Traffic Related Emissions - Brake and Tyre Wear PM - Literature Review. Joint Research Centre, Institute for Energy and Transport. Publications Office of the European Union, Luxembourg. https://data.europa.eu/doi/10.2790/21481.
Hinds, W., 1999. Aerosol Technology. Properties, Behaviour, and Measurement of Airborne Particles, second ed. John Wiley and Sons Inc.
Hopke, P.K., 2016. Review of receptor modeling methods for source apportionment. J. Air Waste Manag. Assoc. 66, 237–259. https://doi.org/10.1080/10962247.2016.1140693.
Hopke, P.K., Dai, Q., Li, L., Feng, Y., 2020. Global review of recent source apportionments for airborne particulate matter. Sci. Total Environ. 740, 140091. https://doi.org/10.1016/j.scitotenv.2020.140091.
IPCC, 2023. Climate Change 2021 – the Physical Science Basis: Working Group I Contribution to the Sixth Assessment Report of the Intergovernmental Panel on Climate Change. Intergovernmental Panel on Climate Change (IPCC). Technical Summary. Cambridge University Press, pp. 35–144. https://doi.org/10.1017/9781009157896.002.
Jayne, J.T., Leard, D.C., Zhang, X., Davidovits, P., Smith, K.A., Kolb, C.E., Worsnop, D.R., 2000. Development of an aerosol mass spectrometer for size and composition analysis of submicron particles. Aerosol Sci. Technol. 33 (1–2), 49–70. https://doi.org/10.1080/027868200410840.
Järvinen, A., Aitomaa, M., Rostedt, A., Keskinen, J., Yli-Ojanperä, J., 2014. Calibration of the new electrical low pressure impactor (ELPI+). J. Aerosol Sci. 69, 150–159. https://doi.org/10.1016/j.jaerosci.2013.12.006.
Karanasiou, A.A., Siskos, P.A., Eleftheriadis, K., 2009. Assessment of source apportionment by Positive Matrix Factorization analysis on fine and coarse urban aerosol size fractions. Atmos. Environ. 43, 3385–3395. https://doi.org/10.1016/j.atmosenv.2009.03.051.
Kim, E., Hopke, P.K., Edgerton, E.S., 2003. Source identification of Atlanta aerosol by positive matrix factorization. J. Air Waste Manag. Assoc. 53 (6), 731–739. https://doi.org/10.1080/10473289.2003.10466209.
Kim, Y., Jeon, K., Park, J., Shim, K., Kim, S.-W., Shin, H.-J., Yi, S.-M., Hopke, P.K., 2022. Local and transboundary impacts of PM2.5 sources identified in Seoul during the early stage of the COVID-19 outbreak. Atmos. Pollut. Res. 13 (8), 101510. https://doi.org/10.1016/j.apr.2022.101510.
Kuo, C.-P., Liao, H.-T., Chou, C.C.-K., Wu, C.-F., 2014. Source apportionment of particulate matter and selected volatile organic compounds with multiple time resolution data. Sci. Total Environ. 472, 880–887. https://doi.org/10.1016/j.scitotenv.2013.11.114.
Lee, D.S., Pacyna, J.M., 1999. An industrial emissions inventory of calcium for Europe. Atmos. Environ. 33 (11), 1687–1697. https://doi.org/10.1016/S1352-2310(98)00286-6.
Li, N., Hopke, P.K., Kumar, P., Cliff, S.S., Zhao, Y.J., Navasca, C., 2013. Source apportionment of time- and size-resolved ambient particulate matter. Chemometr. Intell. Lab. Syst. 129, 15–20. https://doi.org/10.1016/j.chemolab.2013.04.010.
Liao, H.-T., Chou, C.C.-K., Chow, J.C., Watson, J.G., Hopke, P.K., Wu, C.-F., 2015. Source and risk apportionment of selected VOCs and PM2.5 species using partially constrained receptor models with multiple time resolution data. Environ. Pollut. 205, 121–130. https://doi.org/10.1016/j.envpol.2015.05.035.
Liu, T., Tian, Y., Xue, Q., Wei, Z., Qian, Y., Feng, Y., 2018. An advanced three-way factor analysis model (SDABB model) for size-resolved PM source apportionment constrained by size distribution of chemical species in source profiles. Environ. Pollut. 242, 1606–1615. https://doi.org/10.1016/j.envpol.2018.07.118.
Maenhaut, W., Raes, N., Chi, X., Cafmeyer, J., Wang, W., Salma, I., 2005. Chemical composition and mass closure for fine and coarse aerosols at a kerbside in Budapest, Hungary, in spring 2002. X Ray Spectrom. 34 (4), 290–296. https://doi.org/10.1002/xrs.820.
Maenhaut, W., Hillamo, R., Mäkelä, T., Jaffrezo, J.-L., Bergin, M.H., Davidson, C.I., 1996. A new cascade impactor for aerosol sampling with subsequent PIXE analysis. Nucl. Instrum. Methods Phys. Res. B 109–110, 482–487. https://doi.org/10.1016/0168-583X(95)00955-8.
Marigo, M., Zulli, F., Pillon, S., Susanetti, L., De Carli, M., 2022. Heating energy balance and biomass consumption for the residential sector in the Po Valley. Sustain. Energy Technol. Assessment 54, 102814. https://doi.org/10.1016/j.seta.2022.102814.
Marple, V.A., Rubow, K.L., Behm, S.M., 1991. A microorifice uniform deposit impactor (MOUDI): description, calibration, and use. Aerosol Sci. Technol. 14 (4), 434–446. https://doi.org/10.1080/02786829108959504.
Massimi, L., Simonetti, G., Buiarelli, F., Di Filippo, P., Pomata, D., Riccardi, C., Ristorini, M., Astolfi, M., Canepari, S., 2020. Spatial distribution of levoglucosan and alternative biomass burning tracers in atmospheric aerosols, in an urban and industrial hotspot of Central Italy. Atmos. Res. 239, 104904. https://doi.org/10.1016/j.atmosres.2020.104904.
Mason, B., 1966. Principles of geochemistry, 3rd ed. John Wiley and Sons, Inc. Chapter 3.
Mooibroek, D., Sofowote, U.M., Hopke, P.K., 2022. Source apportionment of ambient PM10 collected at three sites in an urban-industrial area with multi-time resolution factor analyses. Sci. Total Environ. 850, 157981. https://doi.org/10.1016/j.scitotenv.2022.157981.
Navarro-Selma, B., Clemente, A., Nicolás, J.F., Crespo, J., Carratalá, A., Lucarelli, F., Giardi, F., Galindo, N., Yubero, E., 2022. Size segregated ionic species collected in a harbour area. Chemosphere 294, 133693. https://doi.org/10.1016/j.chemosphere.2022.133693.
Ng, N.L., Herndon, S.C., Trimborn, A., Canagaratna, M.R., Croteau, P.L., Onasch, T.B., Sueper, D., Worsnop, D.R., Zhang, Q., Sun, Y.L., Jayne, J.T., 2011. An aerosol chemical speciation monitor (ACSM) for routine monitoring of the composition and mass concentrations of ambient aerosol. Aerosol Sci. Technol. 45 (7), 780–794. https://doi.org/10.1080/02786826.2011.560211.
Norris, G., Duvall, R., Brown, S., Bai, S., 2014. EPA Positive Matrix Factorization (PMF) 5.0. Fundamentals and User Guide. U.S. Environmental Protection Agency EPA/600/R-14/108 (NTIS PB2015–105147), Washington, DC.
Ogulei, D., Hopke, P.K., Zhou, L., Paatero, P., Park, S.S., Ondov, J.M., 2005. Receptor modelling for multiple time resolved species: the Baltimore supersite. Atmos. Environ. Times 39 (20), 3751–3762. https://doi.org/10.1016/j.atmosenv.2005.03.012.
Paatero, P., 1999. The multilinear engine: a table-driven, least squares program for solving multilinear problems, including the n-way parallel factor analysis model. J. Comput. Graph Stat. 8 (4), 854–888. https://doi.org/10.2307/1390831.
Paatero, P., Hopke, P.K., 2008. Rotational tools for factor analytic models. J. Chemom. 23 (2), 91–100. https://doi.org/10.1002/cem.1197.

Paatero, P., Hopke, P.K., Song, X.-H., Ramadan, Z., 2002. Understanding and controlling rotations in factor analytic models. Chemometr. Intell. Lab. Syst. 60 (1–2), 253–264. https://doi.org/10.1016/S0169-7439(01)00200-3.

Paatero, P., Tapper, U., 1994. Positive matrix factorization: a non-negative factor model with optimal utilization of error estimates of data values. Environmetrics 5 (2), 111–126. https://doi.org/10.1002/env.3170050203.

Paatero, P., Eberly, S., Brown, S.G., Norris, G.A., 2014. Methods for estimating uncertainty in factor analytic solutions. Atmos. Meas. Tech. 7, 781–797. https://doi.org/10.5194/amt-7-781-2014.

Pant, P., Harrison, R.M., 2013. Estimation of the contribution of road traffic emissions to particulate matter concentrations from field measurements: a review. Atmos. Environ. Times 77, 78–97. https://doi.org/10.1016/j.atmosenv.2013.04.028.

Peré-Trepat, E., Kim, E., Paatero, P., Hopke, P.K., 2007. Source apportionment of time and size resolved ambient particulate matter measured with a rotating DRUM impactor. Atmos. Environ. 41 (28), 5921–5933. https://doi.org/10.1016/j.atmosenv.2007.03.022.

Perrino, C., Catrambone, M., Dalla Torre, S., Rantica, E., Sargolini, T., Canepari, S., 2014. Seasonal variations in the chemical composition of particulate matter: a case study in the Po Valley. Part I: macro-components and mass closure. Environ. Sci. Pollut. Res. 21, 3999–4009. https://doi.org/10.1007/s11356-013-2067-1.

Pietrodangelo, A., Bove, M.C., Forello, A.C., Crova, F., Bigi, A., Brattich, E., Riccio, A., Becagli, S., Bertinetti, S., Calzolai, G., Canepari, S., Cappelletti, D., Catrambone, M., Cesari, D., Colombi, C., Contini, D., Cuccia, E., De Gennaro, G., Genga, A., Ielpo, P., Lucarelli, F., Malandrino, M., Masiol, M., Massabò, D., Perrino, C., Prati, P., Siciliano, T., Tositti, L., Venturini, E., Vecchi, R., 2024. A PM10 chemically characterized nation-wide dataset for Italy. Geographical influence on urban air pollution and source apportionment. Sci. Total Environ. 908, 167891. https://doi.org/10.1016/j.scitotenv.2023.167891.

Pio, C., Casotti Rienda, I., Nunes, T., Gonçalves, C., Tchepel, O., Pina, N.K., Rodrigues, J., Lucarelli, F., Alves, C., 2022. Impact of biomass burning and non-exhaust vehicle emissions on PM10 levels in a mid-size non-industrial western Iberian city. Atmos. Environ. 289, 119293. https://doi.org/10.1016/j.atmosenv.2022.119293.

Polissar, A.V., Hopke, P.K., Paatero, P., Malm, W.C., Sisler, J.F., 1998. Atmospheric aerosol over Alaska: 2. Elemental composition and sources. J. Geophys. Res. 103 (D15), 19045–19057. https://doi.org/10.1029/98JD01212.

Querol, X., Alastuey, A., Viana, M., Moreno, T., Reche, C., Minguillón, M.C., Ripoll, A., Pandolfi, M., Amato, F., Karanasiou, A., Pérez, N., Pey, J., Cusack, M., Vázquez, R., Plana, F., Dall'Osto, M., de la Rosa, J., Sánchez de la Campa, A., Fernández-Camacho, R., Rodrìguez, S., Pio, C., Alados-Arboledas, L., Titos, G., Artíñano, B., Salvador, P., Garcìa Dos Santos, S., Fernández Patier, R., 2013. Variability of carbonaceous aerosols in remote, rural, urban and industrial environments in Spain: implications for air quality policy. Atmos. Chem. Phys. 13, 6185–6206. https://doi.org/10.5194/acp-13-6185-2013.

Reid, J.S., Koppmann, R., Eck, T.F., Eleuterio, D.P., 2005. A review of biomass burning emissions part II: intensive physical properties of biomass burning particles. Atmos. Chem. Phys. 5, 799–825. https://doi.org/10.5194/acp-5-799-2005.

Salma, I., Ocskay, R., Raes, N., Maenhaut, W., 2005. Fine structure of mass size distributions in an urban environment. Atmos. Environ. 39, 5363–5374. https://doi.org/10.1016/j.atmosenv.2005.05.021.

Samara, C., Tsitouridou, R., 2000. Fine and coarse ionic aerosol components in relation to wet and dry deposition. Water Air Soil Pollut. 120, 71–88. https://doi.org/10.1023/A:1005267021828.

Scotto, F., Bacco, D., Lasagni, S., Trentini, A., Poluzzi, V., Vecchi, R., 2021. A multi-year source apportionment of PM2.5 at multiple sites in the southern Po Valley (Italy). Atmos. Pollut. Res. 12 (11), 101192 https://doi.org/10.1016/j.apr.2021.101192.

Seinfeld, J., Pandis, S., 2006. Atmospheric Chemistry and Physics: from Air Pollution to Climate Change, third ed. John Wiley and Sons.

Shi, G.-L., Tian, Y.-Z., Ye, S., Peng, X., Xu, J., Wang, W., Han, B., Feng, Y.-C., 2015. Source apportionment of synchronously size segregated fine and coarse particulate matter, using an improved three-way factor analysis model. Sci. Total Environ. 505, 1182–1190. https://doi.org/10.1016/j.scitotenv.2014.10.106.

Sofowote, U.M., Healy, R.M., Su, Y., Debosz, J., Noble, M., Munoz, A., Jeong, C.-H., Wang, J.M., Hilker, N., Evans, G.J., Hopke, P.K., 2018. Understanding the PM2.5 imbalance between a far and near-road location: results of high temporal frequency source apportionment and parameterization of black carbon. Atmos. Environ. 173, 277–288. https://doi.org/10.1016/j.atmosenv.2017.10.063.

Sofowote, U.M., Mooibroek, D., Healy, R.M., Debosz, J., Munoz, A., Hopke, P.K., 2023. Source apportionment of ambient PM2.5 in an industrialized city using dispersion-normalized, multi-time resolution factor analyses. Environ. Pollut. 323, 121281 https://doi.org/10.1016/j.envpol.2023.121281.

Sofowote, U.M., Healy, R.M., Su, Y., Debosz, J., Noble, M., Munoz, A., Jeong, C.-H., Wang, J.M., Hilker, N., Evans, G.J., Brook, J.R., Lu, G., Hopke, P.K., 2021. Sources, variability and parameterizations of intra-city factors obtained from dispersion-normalized multi-time resolution factor analyses of PM2.5 in an urban environment. Sci. Total Environ. 761, 143225 https://doi.org/10.1016/j.scitotenv.2020.143225.

Srivastava, D., Favez, O., Petit, J.-E., Zhang, Y., Sofowote, U.M., Hopke, P.K., Bonnaire, N., Perraudin, E., Gros, V., Villenave, E., Albinet, A., 2019. Speciation of organic fractions does matter for aerosol source apportionment. Part 3: Combining off-line and on-line measurements. Sci. Total Environ. 690, 944–955. https://doi.org/10.1016/j.scitotenv.2019.06.378.

Stein, A.F., Draxler, R.R., Rolph, G.D., Stunder, B.J.B., Cohen, M.D., Ngan, F., 2015. NOAA's HYSPLIT atmospheric transport and dispersion modeling system. Bull. Am. Meteorol. Soc. 96, 2059–2077. https://doi.org/10.1175/BAMS-D-14-00110.1.

Thorpe, A., Harrison, R.M., 2008. Sources and properties of non-exhaust particulate matter from road traffic: a review. Sci. Total Environ. 400 (1–3), 270–282. https://doi.org/10.1016/j.scitotenv.2008.06.007.

Tian, Y., Harrison, R.M., Feng, Y., Shi, Z., Liang, Y., Li, Y., Xue, Q., Xu, J., 2021. Size-resolved source apportionment of particulate matter from a megacity in northern China based on one-year measurement of inorganic and organic components. Environ. Pollut. 289, 117932. https://doi.org/10.1016/j.envpol.2021.117932.

Tian, S.L., Pan, Y.P., Wang, Y.S., 2016. Size-resolved source apportionment of particulate matter in urban Beijing during haze and non-haze episodes. Atmos. Chem. Phys. 16, 1–19. https://doi.org/10.5194/acp-16-1-2016.

Ulbrich, I.M., Canagaratna, M.R., Cubison, M.J., Zhang, Q., Ng, N.L., Aiken, A.C., Jimenez, J.L., 2012. Three-dimensional factorization of size-resolved organic aerosol mass spectra from Mexico City. Atmos. Meas. Tech. 5, 195–224. https://doi.org/10.5194/amt-5-195-2012.

Varrica, D., Bardelli, F., Dongarrà, G., Tamburo, E., 2013. Speciation of Sb in airborne particulate matter, vehicle brake linings, and brake pad wear residues. Atmos. Environ. 64, 18–24. https://doi.org/10.1016/j.atmosenv.2012.08.067.

Vecchi, R., Piziali, F.A., Valli, G., Favaron, M., Bernardoni, V., 2019. Radon-based estimates of equivalent mixing layer heights: a long-term assessment. Atmos. Environ. Times 197, 150–158. https://doi.org/10.1016/j.atmosenv.2018.10.020.

Vecchi, R., Bernardoni, V., Valentini, S., Piazzalunga, A., Fermo, P., Valli, G., 2018. Assessment of light extinction at a European polluted urban area during wintertime: impact of PM1 composition and sources. Environ. Pollut. 23, 679–689. https://doi.org/10.1016/j.envpol.2017.10.059.

Via, M., Yus-Díez, J., Canonaco, F., Petit, J.-E., Hopke, P., Reche, C., Pandolfi, M., Ivančič, M., Rigler, M., Prévôt, A.S.H., Querol, X., Alastuey, A., Minguillon, M.C., 2023. Towards a better understanding of fine PM sources: online and offline datasets combination in a single PMF. Environ. Int. 177, 108006. https://doi.org/10.1016/j.envint.2023.108006.

Viana, M., Hammingh, P., Colette, A., Querol, X., Degraeuwe, B., de Vlieger, I., van Aardenne, J., 2014. Impact of maritime transport emissions on coastal air quality in Europe. Atmos. Environ. 90, 96–105. https://doi.org/10.1016/j.atmosenv.2014.03.046.

Viana, M., Kuhlbusch, T.A.J., Querol, X., Alastuey, A., Harrison, R.M., Hopke, P.K., Winiwarter, W., Vallius, M., Szidat, S., Prévôt, A.S.H., Hueglin, C., Bloemen, H., Wåhlin, P., Vecchi, R., Miranda, A.I., Kasper-Giebl, A., Maenhaut, W., Hitzenberger, R., 2008. Source apportionment of particulate matter in Europe: a review of methods and results. J. Aerosol Sci. 39 (10), 827–849. https://doi.org/10.1016/j.jaerosci.2008.05.007.

Wexler, A.S., Johnston, M.V., 2008. What have we learned from highly time-resolved measurements during EPA's supersites program and related studies? J. Air Waste Manag. Assoc. 58 (2), 303–319. https://doi.org/10.3155/1047-3289.58.2.303.

WHO global air quality guidelines, 2021. Particulate Matter (PM2.5 and PM10), Ozone, Nitrogen Dioxide, Sulfur Dioxide and Carbon Monoxide. World Health Organization, Geneva. https://www.who.int/publications/i/item/9789240034228.

Wolfenbarger, J.K., Seinfeld, J.H., 1990. Inversion of aerosol size distribution data. J. Aerosol Sci. 21 (2), 227–247. https://doi.org/10.1016/0021-8502(90)90007-K.

Yubero, E., Carratalà, A., Crespo, J., Nicolàs, J., Santacatalina, M., Nava, S., Lucarelli, F., Chiari, M., 2011. PM10 source apportionment in the surroundings of the San Vicente del Raspeig cement plant complex in southeastern Spain. Environ. Sci. Pollut. Res. 18, 64–74. https://doi.org/10.1007/s11356-010-0352-9.

Zhou, L., Hopke, P.K., Paatero, P., Ondov, J.M., Pancras, J.P., Pekney, N.J., Davidson, C. I., 2004. Advanced factor analysis for multiple time resolution aerosol composition data. Atmos. Environ. 38 (29), 4909–4920. https://doi.org/10.1016/j.atmosenv.2004.05.040.